Non-Linear Control of a Six-Phase Floating Interleaved Boost Converter with Coupled Inductors for Fuel Cell Hybrid Power Supply in Heavy-Duty Applications

Niema EL HADDAJI
Université Marie et Louis Pasteur ,UTBM
Institut Femto-ST, FCLAB, CNRS
Belfort, France
niema.elhaddaji@femto-st.fr

Abdesslem DJERDIR
Université Marie et Louis Pasteur ,UTBM
Institut Femto-ST, FCLAB, CNRS
Belfort, France
abdesslem.djerdir@utbm.fr

Serge PIERFEDERICI
Université de Lorraine
LEMTA, CNRS
Vandoeuvre-lès-Nancy, France
serge.pierfederici@univ-lorraine.fr

Daniel HISSEL
Université Marie et Louis Pasteur ,UTBM
Institut Femto-ST, FCLAB, CNRS
Institut Universitaire de France (IUF)
Belfort, France
daniel.hissel@univ-fcomte.fr

***Abstract*—This work is part of a project focused on optimizing the use of fuel cells in heavy-duty transportation systems. It introduces a novel six-phase floating interleaved boost converter (6-FIBC) with coupled inductors, along with its tailored non-linear control strategy, designed for fuel cell hybrid systems in heavy-duty applications. The proposed 6-FIBC topology leverages interleaving techniques and coupled inductors to minimize current ripple, enhance voltage balancing, and boost efficiency. The accompanying non-linear control ensures accurate voltage regulation, stable current sharing, and adaptability to dynamic load variations, optimizing the overall performance of the fuel cell system. Simulation results validate the effectiveness of the proposed structure and control strategy in ensuring system stability, enhancing energy conversion efficiency, and improving overall reliability. Experimental validation is planned to confirm the practical feasibility of the proposed approach.**

***Index Terms*—Fuel Cell, Hybrid Electric Vehicle, DC-DC Power Converter, Boost, Coupled Inductors, Non linear Control.**

I. Introduction

Proton exchange membrane fuel cells (PEMFCs) are a promising technology due to their high energy density and low environmental impact [1]. However, their integration with power electronic converters poses challenges such as dynamic load handling, voltage ripple management, and efficiency optimization, especially in high-power applications like trucks and ships [2]. To address these challenges, floating interleaved boost converters (FIBC) have emerged as an attractive solution for fuel cell systems. Their multi-phase structure reduces input current ripple and distributes power evenly across phases, thereby improving system efficiency and reliability [3], [4], [5].

This study proposes a six-phase floating interleaved boost converter (6-FIBC) with coupled inductors, a novel topology designed to overcome these limitations. The coupled inductors further enhance efficiency by improving magnetic coupling, reducing core losses, and minimizing current ripple [6]. The 6-FIBC topology provides superior performance in terms of voltage regulation and energy conversion efficiency, making it particularly suitable for high-power applications in fuel cell hybrid systems.

In addition to the advanced topology, this work introduces a nonlinear flatness-based control strategy tailored to the 6-FIBC. Flatness-based control enables precise regulation of system states, such as inductor currents and capacitor voltages, while offering dynamic adaptability to varying and cyclic load conditions, as typically encountered in fuel cell applications. This control approach is particularly effective in avoiding current transients during rapid changes in load demand. Unlike conventional linear control methods, which rely on local linearization and may struggle with the system's nonlinear behavior, flatness-based control explicitly incorporates the system's intrinsic dynamics, thereby enhancing robustness and stability under both transient and steady-state conditions. It also facilitates feedforward control design, improving dynamic response and minimizing overshoot. While the interleaving and magnetic coupling within the 6-FIBC architecture are primarily responsible for reducing input current ripple, the proposed control strategy ensures accurate tracking of reference

This work was supported by the EIPHI Graduate School (Contract ANR-17-EURE-0002) and the Region Bourgogne Franche-Comté. The HYSySPEM project was funded by the "France 2030" government investment plan managed by the French National Research Agency, under the reference "ANR-22-PEHY-0018

trajectories and maintains voltage regulation across interleaved phases [7], [8], [9].

This combination of an innovative converter topology and advanced control methodology addresses critical challenges in fuel cell systems, including efficient power transfer, reduced energy losses, and reliable operation. Simulation results validate the effectiveness of the proposed system, demonstrating its capability to achieve superior voltage regulation, balanced current sharing, and enhanced efficiency under dynamic operating conditions.

The remainder of this paper is organized as follows: Section II presents the proposed six-phase floating interleaved boost converter (6-FIBC) with coupled inductors, including its topology, mathematical modeling, and the associated nonlinear flatness-based control strategy. Section III provides simulation results to evaluate the system's performance under both steady-state and dynamic load conditions. Finally, Section IV concludes the paper and outlines directions for future experimental validation.

II. 6-Phase Floating Interleaved Boost Converter with Coupled Inductors

A. Presentation of the converter

To satisfy the requirements of the specification, this study utilizes a 6-FIBC with coupled inductors as shown in Fig.1. The design includes two cascaded modules: a non-floating interleaved module at the top and a floating module at the bottom. Both modules operate with a three-phase interleaved boost converter [10], sharing a common input voltage and dividing their output across the load.

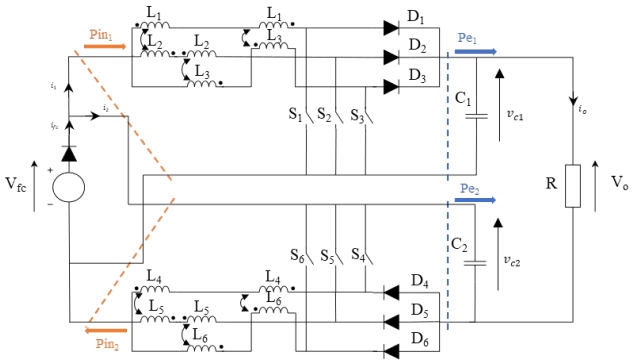

Fig 1. 6-FIBC

The system includes the main switches (S_1 to S_6), diodes (D_1 to D_6), coupled inductors (L_1 to L_6), output capacitors (C_1, C_2), and load resistance (R). The input voltage (v_{fc}) is provided by the PEMFC, with the output voltage (v_o) divided across v_{c1} and v_{c2}.

The proposed 6-FIBC is sized for a Ballard 63 kW FCgen-LCS stack, which serves as the elementary unit of the Ballard FCwave module, a high-power fuel cell system designed for demanding applications [11]. This ensures full compatibility with the selected PEMFC system.

With an input voltage ranging from 176 V to 224 V and an output voltage of 800 V, the converter steps up the fuel cell voltage to meet the DC-link requirements of the vehicle's powertrain, ensuring stable operation despite input variations. The interleaved architecture minimizes current ripple, reducing stress on the fuel cell and enhancing system efficiency.

If adaptation to other power levels is required, the passive component values— inductors and capacitors—must be adjusted accordingly, while the converter topology and control strategy remain unchanged, making it scalable for various fuel cell applications.

B. Converter Modeling

Through the application of Kirchhoff's law, the expressions governing voltage and current within the circuit are

$$\begin{aligned} v_o &= v_{c1} + v_{c2} - v_{fc} \\ i_1 &= i_{L1} + i_{L2} + i_{L3} \\ i_2 &= i_{L4} + i_{L5} + i_{L6} \\ i_{fc} &= i_1 + i_2 - i_o \end{aligned} \tag{1}$$

Where i_1 is the current flowing through the non-floating part, and i_2 flows through the floating part. Here, i_{Ln} for $n = 1...6$ represents the current through inductor L_n (1 to 6).

Assuming symmetry in the converter, the parameters are equalized as follows to maintain balance across all phases and ensure uniform power distribution

$$\begin{aligned} L_1 = \cdots = L_6 = L \\ C_1 = C_2 = C \end{aligned} \tag{2}$$

When a switch S_i (where $i = 1, \ldots, 6$) is ON ($u_i = 1$), the input source charges the inductor, and the capacitor supplies the load.

$$v_{L_{ON}} = v_{fc} \tag{3}$$

When S_i is OFF ($u_i = 0$), the input source and inductor together charge the capacitor and supply the load.

$$v_{L_{OFF}} = v_{fc} - v_o \tag{4}$$

In the 6-FIBC, inductors are coupled to enhance current sharing, reduce ripple, and improve overall efficiency. Instead of employing six independent inductors, mutual inductance is introduced between phases to influence the inductor behavior. A *cascaded cyclic coupling* scheme is implemented, following a structured pattern where each inductor is divided into two parts, with each part magnetically coupled to the next in the sequence, except for the first and last inductors, which are linked together to complete the cyclic structure. This coupling strategy ensures balanced energy distribution, enhances ripple cancellation while maintaining circuit symmetry.

Based on the coupling structure and the symmetry assumptions, the dynamic behavior of the system can be written in compact matrix form as shown in equations (5a), (5b), and (5c).

$$\begin{bmatrix} \dot{i}_{L1} \\ \dot{i}_{L2} \\ \dot{i}_{L3} \end{bmatrix} = \begin{bmatrix} 2L & -M & -M \\ -M & 2L & -M \\ -M & -M & 2L \end{bmatrix}^{-1} (v_{fc} - (I - \mathbf{d}_1)v_{C1}) \tag{5a}$$

$$\begin{bmatrix} \dot{i}_{L4} \\ \dot{i}_{L5} \\ \dot{i}_{L6} \end{bmatrix} = \begin{bmatrix} 2L & -M & -M \\ -M & 2L & -M \\ -M & -M & 2L \end{bmatrix}^{-1} (v_{fc} - (I - \mathbf{d}_2)v_{C2}) \tag{5b}$$

$$\begin{aligned} C \cdot \dot{v}_{C1} &= (1 - \mathbf{d}_1)^T \cdot i_1 - i_o \\ C \cdot \dot{v}_{C2} &= (1 - \mathbf{d}_2)^T \cdot i_2 - i_o \end{aligned} \tag{5c}$$

Where

$$i_1 = \begin{bmatrix} i_{L1} \\ i_{L2} \\ i_{L3} \end{bmatrix}, \quad i_2 = \begin{bmatrix} i_{L4} \\ i_{L5} \\ i_{L6} \end{bmatrix},$$

$$\mathrm{d}_1 = \begin{bmatrix} d_1 \\ d_2 \\ d_3 \end{bmatrix}, \quad \mathbf{d}_2 = \begin{bmatrix} d_4 \\ d_5 \\ d_6 \end{bmatrix}, \quad I = \begin{bmatrix} 1 & 0 & 0 \\ 0 & 1 & 0 \\ 0 & 0 & 1 \end{bmatrix}$$

M represents the mutual inductances, and for maintaining the symmetrical balance of the circuit like all the other parameters.

M is preceded by a minus sign $(-)$, which refers to the inverse coupling. The coupling coefficient is given by $k = \frac{M}{L}$.

C. Converter Control

The control strategy for the 6-FIBC with coupled inductors comprises a power control loop and a current control loop, as shown in Fig. 2. The power control loop generates reference currents, while the current control loop adjusts the duty cycles to ensure balanced and efficient operation.

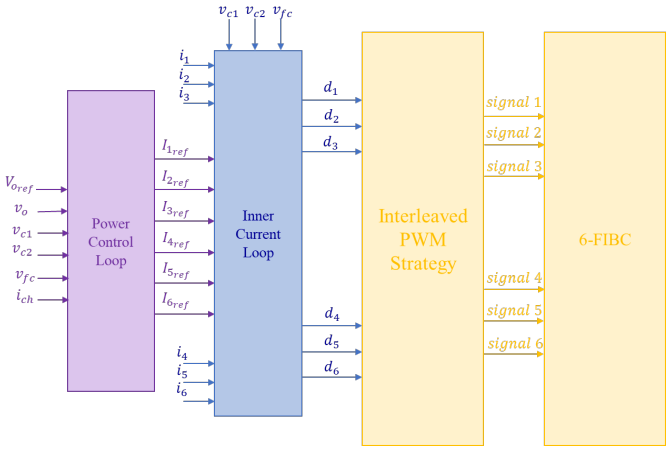

Fig 2. Control Block Diagram

1) Outer Control Loop: This loop regulates the output voltages V_{c1} and V_{c2} of the 6-FIBC with coupled inductors by managing the electrostatic energy stored in the output capacitors C_1 and C_2. The control variables P_{e1} and P_{e2} are used to achieve this regulation.

The electrostatic energy terms y_{o1} and y_{o2} are selected as flat output candidates, satisfying the first flatness condition, and are defined as

$$\begin{aligned} y_{o1} &= \frac{1}{2}C(v_{c1}^2 + v_{c2}^2) = \phi(x) \\ y_{o2} &= \frac{1}{2}C(v_{c1}^2 - v_{c2}^2) = \phi(x) \end{aligned} \tag{7}$$

Where $\mathbf{x} = \begin{bmatrix} x_1 = V_{c1}, & x_2 = V_{c2} \end{bmatrix}$

The second flatness condition is verified by expressing the states as functions of the flat outputs

$$\begin{aligned} v_{c1} &= \sqrt{\frac{2y_{o1}}{C}} \\ v_{c2} &= \sqrt{\frac{2y_{o2}}{C}} \end{aligned} \tag{8}$$

To establish the relationship between power and flat outputs, the derivatives $\dot{y}_{o1}$ and $\dot{y}_{o2}$ are utilized as defined by the following equation

$$\begin{aligned} \dot{y}_{o1} &= P_{o1} - P_{ch1} \\ \dot{y}_{o2} &= P_{o2} - P_{ch2} \end{aligned} \tag{9}$$

Where

$$\begin{aligned} P_{o1} &= (P_{e1} + P_{e2}) \\ P_{o2} &= (P_{e1} - P_{e2}) \end{aligned} \tag{10}$$

and P_{ch1} and P_{ch2} are defined as

$$\begin{aligned} P_{ch1} &= (v_{c1} + v_{c2}) \cdot i_o \\ P_{ch2} &= (v_{c1} - v_{c2}) \cdot i_o \end{aligned} \tag{11}$$

P_{e1} and P_{e2} represent the electrostatic power delivered to the output capacitors C_1 and C_2, respectively, as shown in Fig. 1.

Then, the sum of input powers at the input of each stage can be obtained thanks to

$$P_{in1} + P_{in2} = 2P_{\max}\left(1 - \sqrt{1 - \frac{P_{\text{oref}}}{P_{\max}}}\right) \tag{12}$$

where

$$\begin{aligned} P_{\max} &= \frac{V_e^2}{4 \cdot (2r/6)} \\ P_{\text{oref}} &= P_{\text{o1}} + P_{\text{o2}} \end{aligned} \tag{13}$$

In practice, this expression is not used in the implementation. Instead, the fuel cell power is directly set to the reference value, i.e., $P_{\text{fc}} = P_{\text{o1}} - v_{fc}.i_o$, under the assumption that Joule losses are negligible and are compensated by the integral term in the control loop.

Trajectory Tracking for the flat outputs y_{o1} and y_{o2} is achieved with control laws

$$P_{o1} - (P_{ch1} + P_{ch2}) = \dot{y}_{o1} = \dot{y}_{o1_{\text{ref}}} + k_{v1}(y_{o1} - y_{o1_{\text{ref}}}) + k_{v2} \int (y_{o1} - y_{o1_{\text{ref}}})\, dt = 0,$$

$$P_{o2} - (P_{ch1} - P_{ch2}) = \dot{y}_{o2} = \dot{y}_{o2_{\text{ref}}} + k_{v1}(y_{o2} - y_{o2_{\text{ref}}}) + k_{v2} \int (y_{o2} - y_{o2_{\text{ref}}})\, dt = 0. \tag{14}$$

Where $V_{c1,ref}$ and $V_{c2,ref}$ are the desired reference voltages

$$\begin{aligned} y_{o1,ref} &= \frac{1}{2} C (V_{c1,ref}^2 + V_{c2,ref}^2) \\ y_{o2,ref} &= \frac{1}{2} C (V_{c1,ref}^2 - V_{c2,ref}^2) \end{aligned} \tag{15}$$

and

$$k_{v1} = 2\xi\omega_0, \quad k_{v2} = \omega_0^2 \tag{16}$$

The control gains k_{v1} and k_{v2} were selected to achieve a critically damped response and minimal overshoot.

Thus, from 10, P_{e1} and P_{e2} are expressed as

$$\begin{aligned} P_{in1} = P_{e1} &= \frac{P_{o1} + P_{o2}}{2} \\ P_{in2} = P_{e2} &= \frac{P_{o1} - P_{o2}}{2} \end{aligned} \tag{17}$$

The input reference currents i_{ref_1} to i_{ref_6} are computed based on the distributed powers P_{e1} and P_{e2}. If the total effective power exceeds the maximum current limit

$$I_{\max} = \frac{i_{fc}}{6} \tag{18}$$

the currents are all equal to $I_{\max}$. Otherwise, assuming the losses are negligible, the reference currents are calculated as

$$i_{ref_i} = \max\left(0, \frac{P_{in_i}}{3 v_{fc}}\right) \tag{19}$$

This ensures balanced power distribution across the converter phases while maintaining current and voltage regulation.

2) Inner Control Loop: This loop uses the inductor currents i_{L1} to i_{L6} as flat output candidates, grouped into two sets

$$I_{L1} = [i_1, i_2, i_3]^T, \quad I_{L2} = [i_4, i_5, i_6]^T \tag{20}$$

These currents satisfy the flatness conditions, enabling the duty cycles (D_1, D_2) to be expressed as functions of the inductor currents and their derivatives. The dynamics of the inductor currents are described as

$$\begin{aligned} \frac{dI_{L1}}{dt} &= L^{-1}[v_{fc} I - r_t I_{L1} - (1 - D_1) V_{c1}] \\ \frac{dI_{L2}}{dt} &= L^{-1}[v_{fc} I - r_t I_{L2} - (1 - D_2) V_{c2}] \end{aligned} \tag{21}$$

where

$$I = [1, 1, 1]^T \tag{22}$$

and

$$L = \begin{bmatrix} 2L & -M & -M \\ -M & 2L & -M \\ -M & -M & 2L \end{bmatrix} \tag{23}$$

and

$$D_1 = [d_1, d_2, d_3]^T, \quad D_2 = [d_4, d_5, d_6]^T \tag{24}$$

A second order control law is defined to ensure a good reference tracking

$$\frac{d}{dt}(I_{ref} - i_l) + K_{i1}(I_{ref} - i_l) + K_{i2} \int (I_{ref} - i_l) = 0 \tag{25}$$

Hence, the duty cycles are calculated through

$$\begin{aligned} DD_1 = I + \frac{1}{V_{c1}} [ri - v_{fc} \cdot I + L \frac{di_{\text{ref}}}{dt} + LK_{i1}(I_{\text{ref}} - I_{l1})] \\ + LK_{2i} \int (I_{\text{ref}} - I_{l1})\, dt, \end{aligned}$$

$$\begin{aligned} D_2 = I + \frac{1}{V_{c2}} [ri - v_{fc} \cdot I + L \frac{di_{\text{ref}}}{dt} + LK_{i1}(I_{\text{ref}} - I_{l2})] \\ + LK_{2i} \int (I_{\text{ref}} - I_{l2})\, dt. \end{aligned} \tag{26}$$

Where

$$k_{i1} = 2\xi\omega_0, \quad k_{i2} = \omega_0^2 \tag{16}$$

In contrast to conventional linear control methods based on frequency-domain analysis (e.g., Bode plots), the proposed nonlinear flatness-based control computes system inputs via differential parametrization [12], inherently constraining system poles along a desired trajectory to ensure stability. This removes the need for loop-shaping, as stability is instead evaluated through closed-loop response and reference tracking. The control architecture comprises two decoupled loops: a fast inner loop regulating inductor currents and a slower outer loop managing capacitor voltages. This structure improves disturbance rejection by allowing the inner loop to stabilize current dynamics before outer-loop intervention. Furthermore, system behavior remains independent of the operating point [13], ensuring robust performance under varying conditions.

III. Simulation Results

To evaluate the performance of the proposed controller, simulations were conducted using MATLAB/Simulink, with the converter specifications summarized in Table I.

The simulations were performed using a continuous-time solver to accurately capture system dynamics, while real-time implementation will involve discrete-time control on a digital signal processor (DSP). Given that both control loops operate with sampling frequencies significantly higher than their respective bandwidths—approximately $\omega_s/10$ for the inner current loop and $\omega_s/100$ for the outer voltage loop—discretization

TABLE I
CONVERTERS RATED PARAMETERS

Parameters	Value	Unit
Output Voltage (V_o)	800	V
Input Voltage (V_{fc})	176	V
Switching Frequency (f_s)	80	kHz
Inductor (L, r_L)	(122, 0.2)	(μH, mΩ)
Capacity (C)	80	μF
Coupling Coefficient (k)	-0.3	-
Tolerated Output Voltage Ripple (ΔV_o)	$\leq$10%	-
Tolerated Input Current Ripple (ΔI_{fc})	$\leq$10%	-

effects are expected to be negligible, ensuring stable closed-loop performance. Furthermore, since the highest frequency component of the system dynamics remains well below the Nyquist frequency ($\omega_s/2$), the Shannon sampling theorem is not a limiting factor in this case.

To validate the robustness of the system under load disturbances (regulation performance), multiple step changes in the load current were introduced. Fig. 3 shows the resulting voltage response.

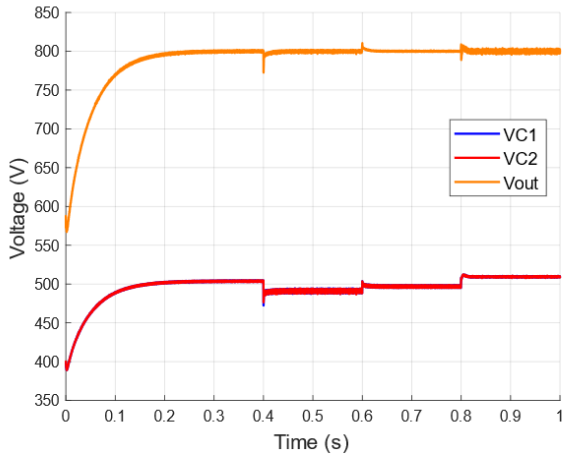

Fig 3. Voltage response under load variations

As shown in Fig. 3, the proposed control strategy maintains tight voltage regulation despite abrupt changes in load demand.

The capacitor voltages v_{c1} and v_{c2} remain balanced around 480 V, while the total output voltage v_o quickly returns to 800 V with minimal overshoot and a fast settling time. The input current i_{fc} adapts effectively, demonstrating good dynamic response and proper power distribution among the interleaved phases.

Fig. 4 illustrates the inductor current profiles i_{L1} to i_{L6}. The interleaved structure enables evenly shared current across all phases, with a maximum deviation of less than 10%. Despite load transients, current ripple remains well-contained, confirming that the control strategy ensures reliable current balancing.

To evaluate tracking performance (reference-following capability), the DC-bus voltage reference was deliberately varied. Fig. 5 illustrates the response of V_{dc} to a sequence of step changes in the reference value.

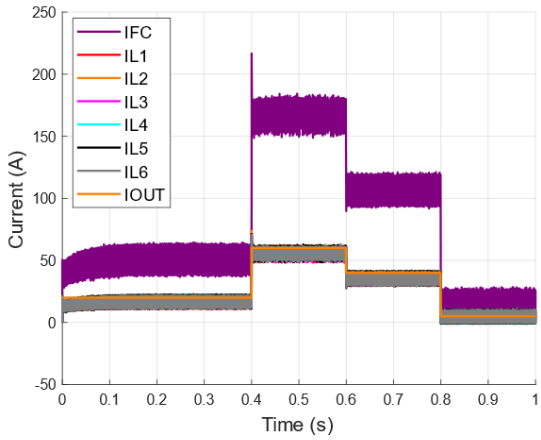

Fig 4. Current response under load variations

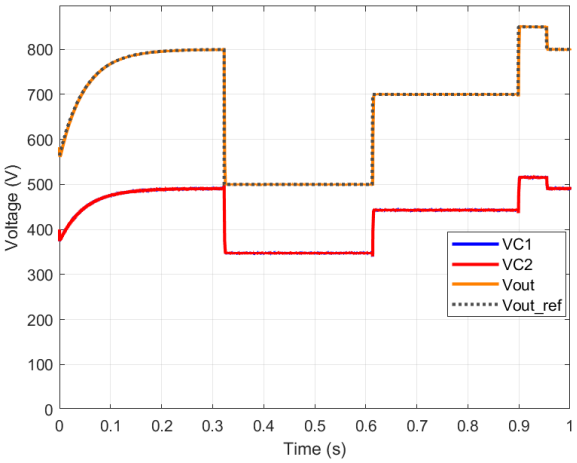

Fig. 5. DC bus voltage tracking performance

The output voltage closely follows the reference throughout all transitions, with minimal overshoot and negligible steady-state error. This highlights the flatness-based controller's effectiveness in dynamic tracking, making it well suited for applications requiring adjustable DC-bus levels, such as multi-source energy coordination or varying load conditions.

Additionally, the system does not exhibit a slow startup, but rather follows a controlled ramp-up process. As shown in Fig. 5, V_{dc} increases progressively by tracking a smoothly rising reference $V_{\text{dc,ref}}$, ensuring safe and stable initialization without abrupt voltage transitions.

IV. CONCLUSION

This work demonstrated the effectiveness of the proposed flatness-based nonlinear control strategy for the six-phase floating interleaved boost converter (6-FIBC) with coupled inductors in achieving stable voltage regulation, balanced current sharing, and efficient energy transfer in fuel cell hybrid systems. Simulation results validated the controller's performance under both nominal and dynamic load conditions, highlighting its robustness, adaptability, and precise

power tracking capabilities. The detailed converter modeling and flatness-based control design contributed to fast transient response, low current ripple, and minimal steady-state error.

While this study focused on simulation-based validation, experimental implementation is planned as future work. The upcoming experimental phase will enable real-time testing of the proposed control approach and converter architecture under practical conditions, providing further insights into hardware performance, control robustness, and system reliability for high-power transportation applications.

REFERENCES

[1] P. Moldrik and R. Chvalek, "Pem fuel cells — the basic characteristics," *2011 10th International Conference on Environment and Electrical Engineering*, pp. 1–4, 2011.

[2] P. Majecki, L. Cavanini, and M. J. Grimble, "Energy optimization strategies for zero emission heavy duty vehicles," *2024 UKACC 14th International Conference on Control (CONTROL)*, pp. 213–218, 2024.

[3] S. Zhuo, A. Gaillard, D. Paire, E. Breaz, and F. Gao, "Design and control of a floating interleaved boost dc-dc converter for fuel cell applications," *IECON 2018 - 44th Annual Conference of the IEEE Industrial Electronics Society*, pp. 2026–2031, 2018.

[4] D. Coutellier, V. G. Agelidis, and S. Choi, "Experimental verification of floating-output interleaved-input dc-dc high-gain transformer-less converter topologies," *2008 IEEE Power Electronics Specialists Conference*, pp. 562–568, 2008.

[5] H. Hidalgo, N. Vázquez, R. Orosco, H. Huerta-Avila, S. Pinto, and L. Estrada, "Floating interleaved boost converter with zero-ripple input current using variable inductor," *Technologies*, 2023.

[6] D. Ciftci, A. Akyildiz, B. E. Ergun, and M. O. Gulbahce, "A comparative study for interleaved boost converter with coupled/uncoupled inductors," *2023 14th International Conference on Electrical and Electronics Engineering (ELECO)*, pp. 1–5, 2023.

[7] Z. Shahrouei, M. Rahmati, R. Gavagsaz-Ghoachani, M. Phattanasak, J.-P. Martin, and S. Pierfederici, "Robust flatness-based control with nonlinear observer for boost converters," *IEEE Transactions on Transportation Electrification*, vol. 9, no. 1, pp. 142–155, 2022.

[8] M. Soheil-Hamedani, M. Zandi, R. Gavagsaz-Ghoachani, B. Nahid-Mobarakeh, and S. Pierfederici, "Flatness-based control method: A review of its applications to power systems," in *2016 7th Power Electronics and Drive Systems Technologies Conference (PEDSTC)*. IEEE, 2016, pp. 547–552.

[9] A. Houari, H. Renaudineau, J.-P. Martin, S. Pierfederici, and F. Meibody-Tabar, "Flatness-based control of three-phase inverter with output lc filter," *IEEE Transactions on Industrial Electronics*, vol. 59, no. 7, pp. 2890–2897, 2011.

[10] M. Harimon, A. Ponniran, A. Kasiran, and H. Hamzah, "A study on 3-phase interleaved dc-dc boost converter structure and operation for input current stress reduction," *Int. J. Power Electron. Drive Syst*, vol. 8, no. 4, pp. 1948–1953, 2017.

[11] B. P. Systems, "Fcwave™ fuel cell power module – technical specification," 2024, accessed: March 2025. [Online]. Available: https://www.ballard.com

[12] M. Fliess, J. Lévine, P. Martin, and P. Rouchon, "Flatness and defect of non-linear systems: introductory theory and examples," *International journal of control*, vol. 61, no. 6, pp. 1327–1361, 1995.

[13] P. Rouchon and M. Fliess, "Flatness-based control of nonlinear systems: Design and implementation," in *International Symposium on Nonlinear Control Systems (NOLCOS)*, 2000.